



# A Thermodynamic Method for the Estimation of Free Gas Proportion in Depressurization Production of Natural Gas Hydrate

Shouding Li<sup>1,2,3\*</sup>, Yiming Sun<sup>1,2,3</sup>, Cheng Lu<sup>4,5</sup>, Weichang Chen<sup>1,2,3</sup>, Shimin Liu<sup>6</sup>, Lin Chen<sup>7,8</sup> and Xiao Li<sup>1,2,3</sup>

<sup>1</sup>Key Laboratory of Shale Gas and Geoengineering, Institute of Geology and Geophysics, Chinese Academy of Sciences, Beijing, China, <sup>2</sup>Innovation Academy for Earth Science, Chinese Academy of Sciences, Beijing, China, <sup>3</sup>College of Earth and Planetary Sciences, University of Chinese Academy of Sciences, Beijing, China, <sup>4</sup>Guangzhou Marine Geological Survey, China Geological Survey, Guangzhou, China, <sup>5</sup>Center of Oil and Natural Gas Resource Exploration, China Geological Survey, Beijing, China, <sup>6</sup>Department of Energy and Mineral Engineering, G<sup>3</sup> Center and Energy Institute, The Pennsylvania State University, University Park, State College, PA, United States, <sup>7</sup>Institute of Engineering Thermophysics, Chinese Academy of Sciences, Beijing, China, <sup>8</sup>School of Aeronautics and Astronautics, University of Chinese Academy of Sciences, Beijing, China

## OPEN ACCESS

### Edited by:

Jinan Guan,  
Guangzhou Institute of Energy  
Conversion (CAS), China

### Reviewed by:

Lele Liu,  
Qingdao Institute of Marine Geology  
(QIMG), China  
Zhichao Liu,  
China University of Geosciences  
Wuhan, China  
Guangrong Jin,  
Guangzhou Institute of Energy  
Conversion (CAS), China

### \*Correspondence:

Shouding Li  
lsdiyh@mail.iggcas.ac.cn

### Specialty section:

This article was submitted to  
Marine Geoscience,  
a section of the journal  
Frontiers in Earth Science

Received: 20 January 2022

Accepted: 07 March 2022

Published: 30 March 2022

### Citation:

Li S, Sun Y, Lu C, Chen W, Liu S,  
Chen L and Li X (2022) A  
Thermodynamic Method for the  
Estimation of Free Gas Proportion in  
Depressurization Production of Natural  
Gas Hydrate.  
Front. Earth Sci. 10:859111.  
doi: 10.3389/feart.2022.859111

Free gas saturation is one of the key factors that affect the overall production behaviors of hydrate reservoirs. For example, different free gas contents could alter the thermal response of hydrate reservoirs to the artificial stimulation and hence change the gas production performance. To investigate whether and how much the hydrate reservoir contains free gas, we proposed a thermodynamic method to calculate the total heat consumption of hydrate dissociation throughout gas production and assess the free gas proportion. Based on the monitoring data of the first offshore hydrate production in Japan, we calculated the total heat consumption and analyzed the contributions of heat convection, heat conduction, and sensible heat during the entire test. The calculation results showed that there is likely to be a certain amount of free gas in the hydrate reservoir in the Eastern Nankai Trough. In addition, the analysis of different heat sources revealed the critical thermodynamic phenomenon in which the reservoir sensible heat was the main source for enthalpy of hydrate dissociation, which consistently contributed more than 95% of the total heat supply during the 6-day production test. The results of this work may help upgrade the production strategy for natural gas hydrates.

**Keywords:** natural gas hydrate, free gas proportion, thermodynamic analysis, heat transfer, hydrate production

## 1 INTRODUCTION

Natural gas hydrates (NGHs), found in permafrost regions and marine continental margin sediments, are crystalline compounds formed by water and natural gas molecules (mainly methane) (Kvenvolden 1988; Sloan 2003; Boswell and Collett 2011). In an ideally saturated methane hydrate, the molar ratio of methane to water is nearly 1:6, that is, equal to a volumetric ratio of about 164 (Kvenvolden 1988). The methane concentration in hydrates is comparable to that of a highly compressed gas (Sloan 2003). Therefore, hydrates need to form in the condition in which hydrate-forming gas is sufficient and both pressure and temperature are conducive to hydrate stability. Otherwise, the hydrate crystal may break down and release methane into the

surrounding water. Whether the gas resource is sufficient or not directly affects the formation of NGH and the volume percentage of gas hydrate in hydrate-bearing sediments (HBSs). The presence of methane within the pressure–temperature stability field for methane gas hydrate is not sufficient to ensure the occurrence of gas hydrate, which tends to form when the mass fraction of methane dissolved in liquid exceeds methane solubility in seawater (Xu and Ruppel 1999) and there is free methane gas in the fluid system (Ben Clennell et al., 1999; Waite et al., 2009; Lu et al., 2019). Accordingly, fluid containing methane must rise to the depth at which the local solubility limit is less than the methane content in order for hydrate to precipitate (Waite et al., 2009).

NGH reservoirs can be divided into three main classes on the basis of geological features and initial conditions (Moridis et al., 2009), in which NGH indeed generally coexists with free gas (Makogon and Omelchenko 2013; Miyakawa et al., 2014; Li et al., 2016; Ye et al., 2020). Free gas saturation is a key factor that affects the overall production behaviors of marine hydrate deposit, for example, influencing the thermal response of hydrate reservoir to the artificial stimulation and hence altering the gas production performance (Moridis et al., 2007). Generally, when the gas content is lower than the local solubility, the gas dissolves in the pore water and migrates with it. If the gas exceeds the solubility and the amount is small, a small number of bubbles will migrate with the pore fluid in a discrete form. Accordingly, there are two main sources of free gas in the hydrate reservoir. In one case, methane is transported to the hydrate stability zone by dissolving in pore water. In the rising process, due to the gradual decrease of methane solubility, methane precipitates from water. In another case, methane is directly provided by the fluid containing saturated methane and free gas (Lu et al., 2019). These imply that there is supposed to be a certain proportion of free gas in the hydrate reservoir. Understanding the free gas content of a reservoir will help to establish a hydrate accumulation model and formulate the corresponding production strategy, such as heat-supply strategy and depressurization strategy. However, the evidence of whether and how much the hydrate reservoir contains free gas is scarce, and the method to assess the overall free gas content in a hydrate reservoir is deficient and needs to be developed.

In this article, we proposed a thermodynamic method using real-world production data to calculate the heat consumption of hydrate dissociation in gas production and ultimately evaluate the free gas content in a hydrate reservoir. Taking the first offshore hydrate production of Japan as an example, we conducted the estimation and analyses of free gas proportion in the test reservoir using the on-site monitoring data. Based on this work, we also analyzed the thermal responses of the reservoir and revealed the contributions of different thermal processes. This work will not only conduce to understanding the phase composition of methane gas in hydrate reservoirs but also help us better comprehend the effect of different heat sources in hydrate reservoirs to hydrate dissociation, all of which will better guide future hydrate production.

## 2 PRINCIPLE AND METHOD

The dissociation of methane hydrate is an endothermic process and can significantly change the temperature field in the reservoir (Song et al., 2015; Yamamoto et al., 2017). In contrast, the thermodynamic effect of the release of free gas originally existing in the hydrate reservoir can be ignored. Based on this, we can estimate the heat consumption during gas production according to the thermal response of the formation and then obtain the amount of hydrate-released gas by converting the heat consumption into gas volume. Furthermore, we can calculate the proportion of free gas in the total gas yield.

In the process of gas production, artificial stimulation, such as depressurization, triggers the dissociation, and immediately the hydrate dissociation will absorb heat from the surrounding environment. As the dissociation goes on, a disturbed zone, which can be defined as the zone in which the temperature diverges from the initial state, will expand over time. Consequently, convective water driven by the pressure gradient will be cooled due to heat transfer to the disturbed zone, heat conduction due to the temperature gradient will occur, and sensible heat of the disturbed zone will be released due to formation cooling. In the aforementioned processes, the heat consumption of hydrate dissociation  $Q_h$ , the heat loss of extracted formation water  $Q_w$ , the heat conduction through surrounding formation  $Q_c$ , and the sensible heat released by the disturbed zone  $Q_r$  are the main thermal factors influencing the temperature field (Figure 1). According to the conservation of energy, we can conclude the following relationship (Eq. 1) between these heat items: the heat needed or consumed by hydrate dissociation ( $Q_h$ ) is ultimately derived from and compensated by heat released by formation water ( $Q_w$ ), heat conduction through the disturbed zone ( $Q_c$ ), and sensible heat released by the disturbed zone ( $Q_r$ ). The method of energy balance enables us to ignore the intermediate processes and focus on the change of the thermal field in which the thermal effects of many aspects, such as ice formation and hydrate reformation, will submerge and be reflected in the ultimate temperature states.

$$Q_h = Q_w + Q_c + Q_r. \quad (1)$$

From this point of view, to estimate the free gas content, the first step is to calculate the right-hand members in Eq. 1 and then convert the results into an equivalent volume of hydrate-released gas according to the enthalpy of hydrate dissociation.

In this work, the heat contributed by formation water convection ( $Q_w$ ) in each temporal interval was regarded and calculated as the sensible heat associated with water cooling using Eq. 2:

$$Q_w = c_w \rho_w V_w \Delta t_w, \quad (2)$$

where  $c_w$  and  $\rho_w$  are the specific heat capacity and density of the water, respectively,  $V_w$  is the water production in an interval, and  $\Delta t_w$  is the temperature difference between the real-time temperature and the initial formation temperature.

The heat conduction through the disturbed zone ( $Q_c$ ) is divided into two parts, i.e., the lateral heat conduction from

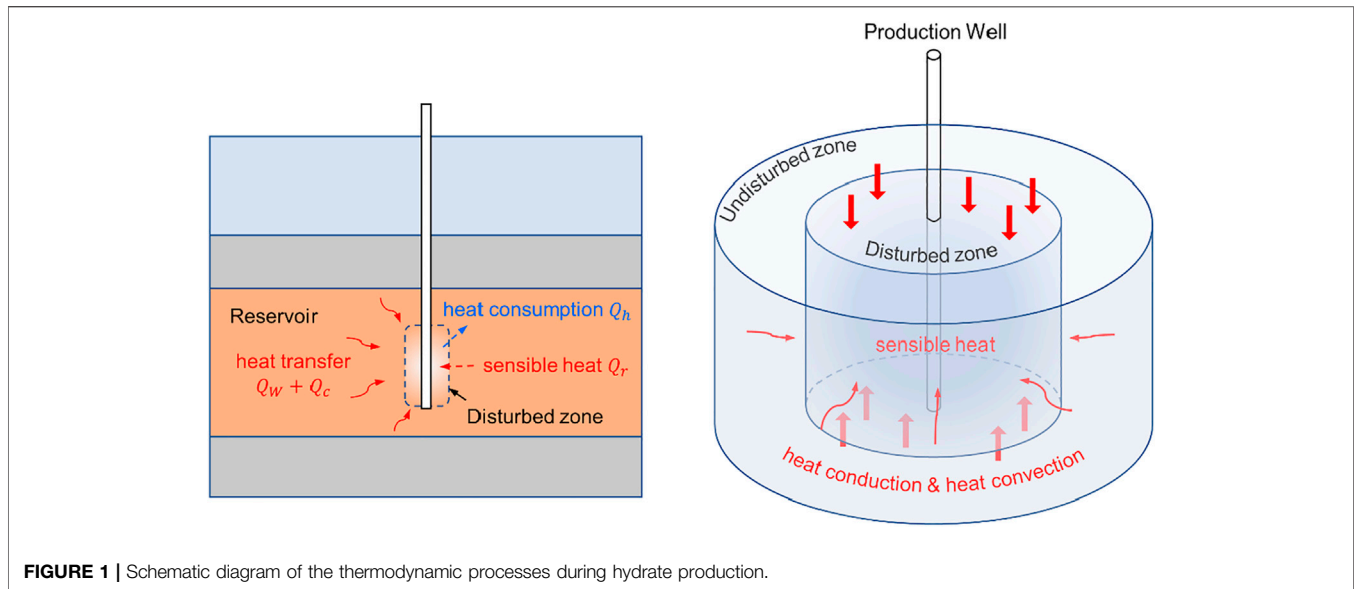


**FIGURE 1** | Schematic diagram of the thermodynamic processes during hydrate production.

the undisturbed zone and the vertical heat conduction from the overburden and underlying layers. In this work, the lateral heat conduction was considered a one-dimension steady heat conduction problem in each temporal interval. As a conventional simplifying method (Li G. et al., 2012; Chen et al., 2018; Yu et al., 2019; Xu et al., 2021), we assumed that the expansion of the disturbed zone approximated to an axisymmetric process in a short-term production, and thus we calculated the corresponding heat using Fourier's law of heat conduction in cylindrical coordinates:

$$\Phi = 2\pi\lambda l \frac{t_1 - t_2}{\ln(r_2/r_1)}, \quad (3)$$

where  $\Phi$  is the heat transfer rate,  $\lambda$  is the thermal conductivity of formation,  $l$  is the height of the cylindrical disturbed zone,  $r_1$  and  $r_2$  are the inner and outer radii of the cylinder, respectively, and  $t_1$  and  $t_2$  are the corresponding boundary temperature. In the geological model,  $r_1$  and  $r_2$  are the radius of wellbore and the radius of the disturbed zone, respectively. By ignoring the effect of the geothermal gradient, the vertical heat conduction was directly calculated using Fourier's law of heat conduction in Cartesian coordinates:

$$\Phi = -2A\lambda\nabla t, \quad (4)$$

where  $A$  is the area of the upper or lower surface of the disturbed zone, and  $\nabla t$  is the temperature gradient in formation.

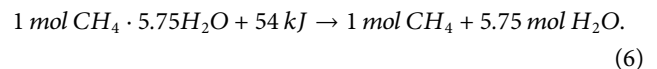
The sensible heat released by the disturbed zone ( $Q_r$ ) can be estimated using the volume of the disturbed zone, the heat capacity of the reservoir, and the temperature difference between the initial and final states according to Eq. 5:

$$Q_r = c_r \rho_r V_r \Delta t_r, \quad (5)$$

where  $c_r$  and  $\rho_r$  are the specific heat capacity and density of formation, respectively,  $V_r$  is the volume of the disturbed zone,

and  $\Delta t_r$  is the temperature change of formation. The equation and calculation will be further detailed later.

With heat consumption calculated, we can estimate the hydrate-released gas by attributing all the heat consumption to the hydrate dissociation. The enthalpy of methane hydrate dissociation  $\Delta H$  can be set at  $54 \text{ kJ mol}^{-1}$  (Handa 1986; Sloan and Koh 2008); therefore, the dissociation equation of methane hydrate can be formulated as



The estimated hydrate-released gas according to Eqs 1,6 is supposed to be less than the gross gas production because of the free gas in the reservoir. Comparing the hydrate-released gas with the gross gas production, we can determine the free gas content in the hydrate deposit. The values and calculations of physical parameters, especially the thermophysical properties will be detailed in the following section.

### 3 CALCULATION AND DISCUSSION

#### 3.1 Data Acquisition and Processing

In March 2013, the world's first field trial of gas production from marine hydrate deposits was conducted in the Daini Atsumi Knoll area of the Eastern Nankai Trough off the Pacific coast of Japan (Yamamoto et al., 2014). One production well AT1-P with two monitoring boreholes, AT1-MC and AT1-MT1, was drilled in the test site. During the entire 6-day flow test, the gas production rate was stable at about  $2.0 \times 10^4 \text{ m}^3 \text{ d}^{-1}$ , with the highest rate of  $2.5 \times 10^4 \text{ m}^3 \text{ d}^{-1}$ . The water production rate was about  $200 \text{ m}^3 \text{ d}^{-1}$ . The cumulative gas production was  $11.9 \times 10^4 \text{ m}^3$ , and water production was  $1,250 \text{ m}^3$  (Konno et al., 2017; Yamamoto et al., 2017). Along with the flow test, the intensive data acquisition program was implemented. DTS and RTD

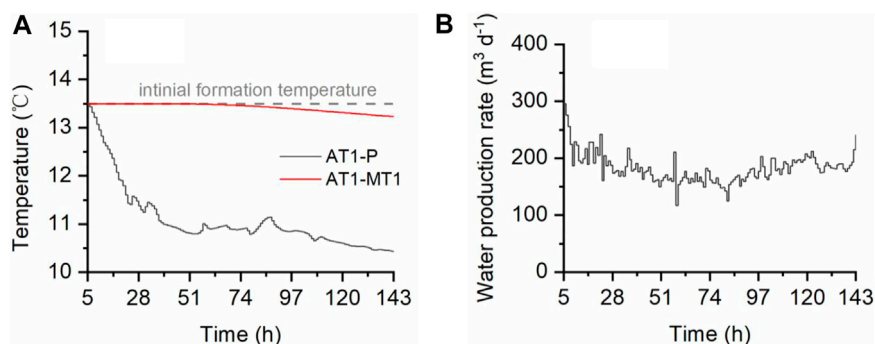


**FIGURE 2** | Data used for calculation. **(A)** Processed downhole temperature data of production well AT1-P and monitoring well AT1-MT1 from the sensor installed 10 m below the top of the methane hydrate-concentrated zone. **(B)** Processed water production data from production well AT1-P.

temperature sensors installed along the production and two observation boreholes detected temperature variations caused by the endothermic dissociation process and heat transfer around the boreholes during gas production.

As the first offshore hydrate production test of Japan provided an integral dataset that recorded the production behavior and reservoir response during the entire depressurization production, in this work, we attempted to take this pilot production as an example and assess the free gas content in the test reservoir. To conduct the calculation in a unified geometry of the model, we simplified the temperature profile in the reservoir via average temperature in our calculations, which should be acceptable given the linear relationship between the heat items and temperature variation and the thermal independence of other parameters. According to the temperature monitoring data, we chose the data gathered by the sensor installed 10 m below the top of the methane hydrate-concentrated zone, which could typify the temperature variation of different formation intervals, as the average temperature to conduct the calculation. According to the timeline of the major events (Yamamoto et al., 2017), the calculated span was set at 138 h, i.e., from 5 to 143 h after the start of depressurization, when the downhole P-T state reached the phase equilibrium curve of methane hydrate and the depressurization operation terminated, respectively.

The fundamental calculation data, namely, temperature variation and water production, were gathered from the literature of Yamamoto et al. (2017) and processed by overall smoothing and hourly homogenizing, as shown in Figure 2.

## 3.2 Heat Consumption Calculation

### 3.2.1 Heat From Formation Water

In the process of hydrate production, hydrate dissociation will absorb heat from the surrounding environment. Therefore, the temperature of the final produced water, that is, the downhole monitoring temperature of the production well was lower than the initial formation temperature. According to energy conservation, the heat loss of produced water constituted a part of heat sources for hydrate dissociation. The produced water was composed of decomposed hydrate water, *in situ* formation water, and inflow formation water. We assume that

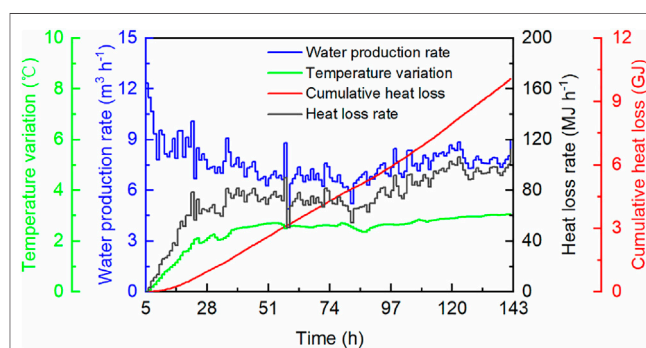
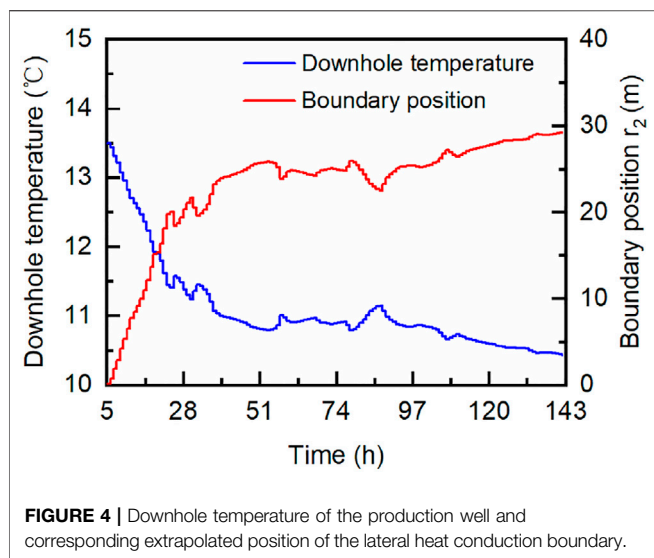


**FIGURE 3** | Calculation results of the heat loss from produced formation water contributing to hydrate dissociation.

the extracted hydrate water and *in situ* water will be replaced by the inflow water, so it can be equivalently considered that they are stationary, and the produced water is equivalent to the inflow water. The heat convection calculation of this part only considers the heat loss of produced water, while the heat loss of hydrate water and *in situ* water is classified into the following sensible heat calculation.

Based on the real-time temperature difference (Figure 2A) and Eq. 2, the heat contributed by formation water can be calculated. The specific heat capacity of seawater was taken as  $4.1 \text{ kJ kg}^{-1} \text{ K}^{-1}$  (Sharqawy et al., 2012; Haynes 2016). Figure 3 gives the temperature variation quantity  $\Delta t_w$  and water production rate, whereby we calculated the item of  $Q_w$ , that is, the heat released by formation water on the hourly basis and obtained a total heat loss of about 10.08 GJ.

Given the discrepancy between the water flux through the boundary of the disturbed zone and the water production rate, for example, the production rate would be bigger than the influx at the beginning in order to decrease the downhole pressure, we carried out the following examination to determine the influence of this issue. Our calculation interval spanned from 5 to 143 h after the start of depressurization, in which the downhole pressure basically hovered between 4.5–5 MPa. The biggest pressure drop of about 6 MPa occurred in the period of



5–12 h. Taking the well diameter as 21.5 cm (8–1/2" drill bit) (Yamamoto et al., 2014), the total introduced error of water volume is about 22 m<sup>3</sup>. Given the temperature drop during this period was less than 1 K, the total corresponding energy error is believed to be about 0.1 GJ, which is 1% of the current calculation results. This shows that the error introduced by the altering of downhole pressure is minor and negligible.

### 3.2.2 Heat From Formation Conduction

The dissociation of hydrates can change the temperature field around the production well, and thus the heat conduction in formation will occur. In this work, the heat conduction through the disturbed zone was simply divided into two parts, that is, the heat from lateral conduction and vertical conduction. The lateral heat conduction was considered a one-dimension steady heat conduction problem in each hourly interval. According to numerical simulations of the short-term hydrate production employing the vertical production well (Yamamoto et al., 2017; Boswell et al., 2019; Feng et al., 2019; Yu et al., 2019), we assumed a cylindrical disturbed zone during the production to calculate the corresponding heat ( $Q_c$ ) using Fourier's law of heat conduction in cylindrical coordinates (Eq. 3). By ignoring the effect of the geothermal gradient, the vertical heat conduction was directly calculated using Fourier's law of heat conduction in Cartesian coordinates (Eq. 4).

Although the calculation model has been simplified, the direct application of Fourier's law is still not feasible because the temperature and position of the internal and external heat conduction boundaries are needed. In the calculation, the temperature at the inner and outer boundaries is known. The former is the temperature data from the production well, and the latter is the initial formation temperature of 13.5°C. The location of the inner boundary, that is, the wellbore radius, is also known, which is 0.1 m (Yamamoto et al., 2017). The biggest obstacle to the calculation lies in the real-time position of the outer conduction boundary. In this hydrate production trial, no instrument could keep track of the boundary of the disturbed zone, that is,  $r_2$  in Eq. 3 was unknown. We tackled this problem in

light of the information provided by the monitoring well AT1-MT1. We noted that the temperature in the AT1-MT1 well, which was 22 m away from the production well, started to manifest a divergence from the initial formation temperature about 30 h after pumping operation. In the meantime, the temperature in the production well was recorded as 11.2°C. Based on the temperature difference and distance between production and monitoring wells, we presumed a linear temperature gradient of 0.1°C m<sup>-1</sup> in the formation in order to extrapolate the lateral position of the heat conduction boundary, as well as the disturbed zone boundary, using the downhole temperature of the production well. The calculation result is shown in Figure 4.

Having the position of the heat conduction boundary in each temporal interval, we can conduct the calculations of lateral conduction and vertical conduction. In Eq. 3, the height  $l$  of the cylindrical disturbed zone was taken as 30 m according to the spatial range of temperature change in the monitoring well during the production test (Yamamoto et al., 2017). The temperature gradient of formation  $\nabla t$  in Eq. 4 also used the value of 0.1°C m<sup>-1</sup>. The thermal conductivity of formation  $\lambda$  was estimated as 1.76 W m<sup>-1</sup> K<sup>-1</sup> using the reservoir parameters (Fujii et al., 2015; Konno et al., 2017; Yamamoto et al., 2017) and the distribution model (Muraoka et al., 2014):

$$\lambda = \lambda_h^{S_h \varphi} \lambda_s^{(1-\varphi)} \lambda_w^{(1-S_h)\varphi}, \quad (7)$$

where  $\lambda_h$ ,  $\lambda_s$ , and  $\lambda_w$  are the thermal conductivities of methane hydrate, sediment grain, and seawater, respectively, and  $S_h$  and  $\varphi$  are the hydrate saturation and porosity of HBS, respectively. This thermal conductivity of formation  $\lambda$  was considered constant irrespective of the temporal and spatial difference caused by the variation of the hydrate saturation in sediments because of the small extent of this difference (Cortes et al., 2009; Waite et al., 2009; Yang et al., 2015; Yang et al., 2016). Figure 5 shows the results of the heat transfer rate in each interval and the cumulative heat contributed by conduction. The heat derived from lateral and vertical heat conduction through formation adds up to about 72.55 and 314.96 MJ, respectively, with a total value of 387.51 MJ.

It should be noted that the calculations of this part were simplified. For instance, the actual temperature profile in the reservoir is bound to be different from the one adopted in the calculation, and the actual geometry of the boundary must not be a simple cylinder. These deficiencies should be overcome in the further study via numerical calculation. But fortunately, the magnitude of the result indicates that the role of heat conduction in the hydrate production is astonishingly insignificant, as the equivalent gas volume of this amount of heat is merely 161 m<sup>3</sup> according to Eq. 6.

### 3.2.3 Sensible Heat Released by the Disturbed Zone

As defined previously and illustrated in Figure 1, the disturbed zone in this work refers to a cylindrical zone in which the temperature diverges from the initial state due to hydrate dissociation and related thermal effect. Figure 4 shows the boundary position of the disturbed zone and the downhole temperature of the production well, whereby the sensible heat associated with the temperature

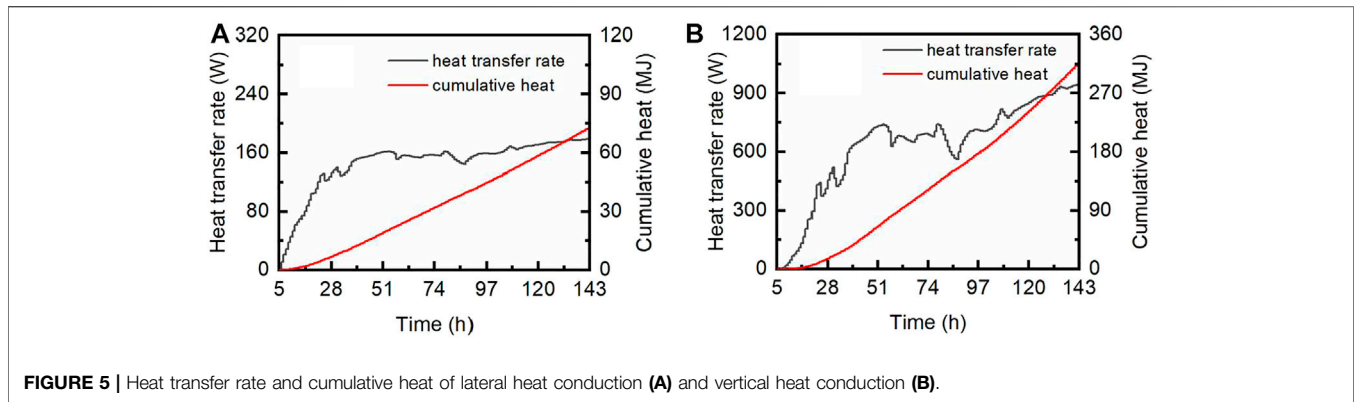


**FIGURE 5** | Heat transfer rate and cumulative heat of lateral heat conduction (A) and vertical heat conduction (B).

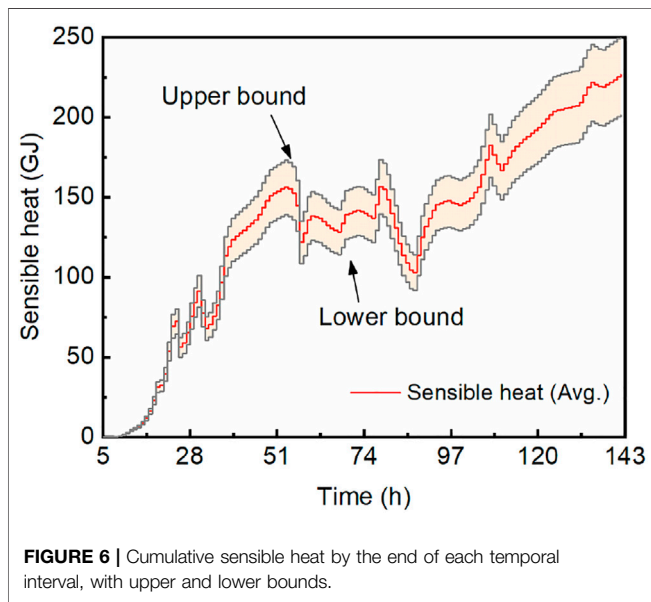


**FIGURE 6** | Cumulative sensible heat by the end of each temporal interval, with upper and lower bounds.

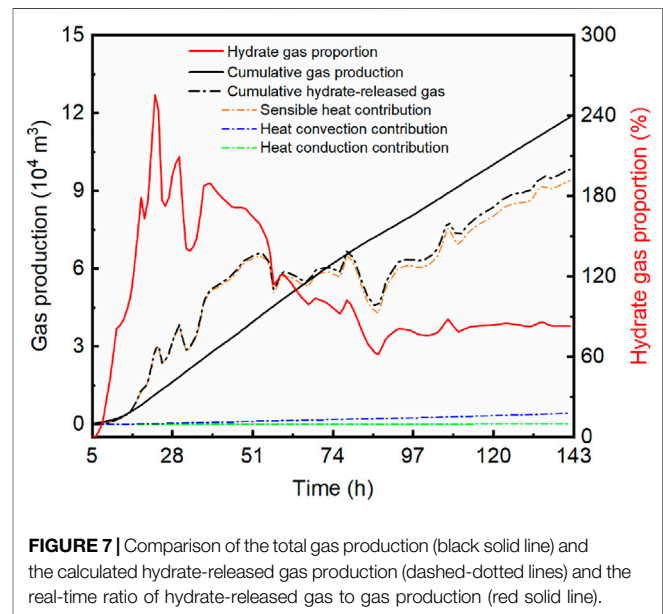


**FIGURE 7** | Comparison of the total gas production (black solid line) and the calculated hydrate-released gas production (dashed-dotted lines) and the real-time ratio of hydrate-released gas to gas production (red solid line).

decrease of formation can be calculated based on Eq. 5. As in Eq. 3, the height  $l$  of the cylindrical disturbed zone was taken as 30 m according to the spatial range of temperature variation in the monitoring well throughout the test (Yamamoto et al., 2017). The volume specific heat  $\rho_r c_r$  of formation is calculated using the arithmetic mean formula:

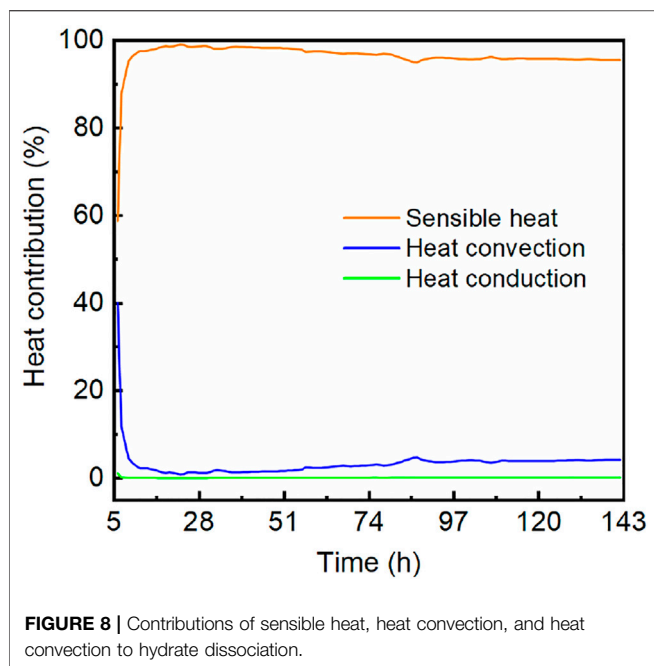
$$\rho_r c_r = \rho_h c_h S_h \varphi + \rho_s c_s (1 - \varphi) + \rho_w c_w (1 - S_h) \varphi, \quad (8)$$

where  $\rho_r$ ,  $\rho_h$ ,  $\rho_s$ , and  $\rho_w$  are the densities of HBS, methane hydrate, sediment grain, and seawater, respectively, and  $c_r$ ,  $c_h$ ,  $c_s$ , and  $c_w$  are the specific heat capacities of the same components. For this calculation,  $\varphi = 40\%$  (Fujii et al., 2015),  $\rho_h = 0.92 \text{ g cm}^{-3}$  (Waite et al., 2007; Muraoka et al., 2014),  $c_h = 2.01 \text{ kJ kg}^{-1} \text{ K}^{-1}$  (Waite et al., 2009; Konno et al., 2010),  $\rho_s = 2.65 \text{ g cm}^{-3}$ ,  $c_s = 0.73 \text{ kJ kg}^{-1} \text{ K}^{-1}$  (Muraoka et al., 2014),  $\rho_w = 1.00 \text{ g cm}^{-3}$ , and  $c_w = 4.11 \text{ kJ kg}^{-1} \text{ K}^{-1}$  (3.5% salinity) (Sharqawy et al., 2012) were considered. The variable is the hydrate saturation  $S_h$ . With the expansion of the dissociation zone, hydrate dissociation may significantly raise the specific heat of HBS, as the specific heat

of methane hydrate is less than that of half of seawater. However, a dynamic calculation with a specific heat varying with time and position is complicated and impracticable. As a compromise in the calculation, the volume-specific heat  $\rho_r c_r$  adopted the mean value of its maximum case  $2.80 \text{ MJ m}^{-3} \text{ K}^{-1}$ , where  $S_h = 0$ , and its minimum case  $2.25 \text{ MJ m}^{-3} \text{ K}^{-1}$ , where  $S_h = 60\%$ , the initial hydrate saturation in the reservoir (Fujii et al., 2015), and the mean value turned out to be  $2.53 \text{ MJ m}^{-3} \text{ K}^{-1}$ , which was regarded as temporally and spatially constant. To calculate the value of  $Q_r$ , Eq. 5 was specified as Eq. 9

$$Q_r = \int_{r_1}^{r_2} \rho_r c_r 2\pi r dr l (\Delta t_r - r \nabla t), \quad (9)$$

based on which the cumulative sensible heats by the end of each temporal interval were calculated. Figure 6 shows the upper bound, average, and lower bound of the sensible heat released by the disturbed zone. The ultimate sensible heat was 226.64 GJ on average, and the upper and lower bounds were 251.25 and 201.75 GJ, respectively.



### 3.3 Free Gas Proportion and Implication

Figure 7 summarizes the calculation results, based on which we can estimate the free gas proportion in the test reservoir using Eqs 1,6. The heat from formation water in total is 10.08 GJ. The heat derived from lateral and vertical heat conduction through the formation adds up to 72.55 and 314.96 MJ, respectively, with a total value of 387.51 MJ. The ultimate sensible heat released by the disturbed zone was 226.64 GJ. Corresponding to these heat items, the equivalent gas volumes are 4,181 m<sup>3</sup>, 161 m<sup>3</sup>, and 94014 m<sup>3</sup>, respectively. These results mean that in 138-h gas production interval, 98356 m<sup>3</sup> of methane gas was generated due to hydrate dissociation. As the total extracted gas was 119000 m<sup>3</sup>, the proportion of free gas in the gross gas yield, or in the test reservoir, was estimated as 17.35%. Considering the variation range of cumulative sensible heat, the maximum and minimum volumes of the total hydrate-released gas would be 108565 m<sup>3</sup> and 88031 m<sup>3</sup>, respectively. The corresponding free gas proportion will be 8.77% and 26.02%, respectively. According to the results, there is likely to be a certain amount of free gas in the NGH deposit in the Eastern Nankai Trough.

In Figure 7 the hydrate gas proportion, namely, the ratio of hydrate-released gas to actual extracted gas, indicates that free gas was first extracted in the beginning of few hours, and then the hydrate dissociation sprang up as the hydrate gas proportion surged in the following hours. The proportion exceeding 100% indicates a delay of gas extraction caused by the sluggish gas migration in low-permeability formation. However, after the delay period, the hydrate gas production represents a declining trend, which may imply a pause of hydrate dissociation and even a reformation phenomenon of hydrates. As the gas extraction went on, the hydrate gas proportion decreased continuously until it converged to a basically stable value of 82.65%.

As an endothermic process, hydrate dissociation will absorb heat from various sources. Our calculation demonstrated that hydrate gas generation was mainly contributed by sensible heat associated with the temperature decrease of formation. As shown in Figure 7, the gas production related to sensible heat accounts for 95.6% of the total hydrate-released gas. Figure 8 shows the contributions of the three heat items to hydrate dissociation. In the first few hours, both the sensible heat and heat convection constituted the main heat source to hydrate dissociation, but then they evolved toward opposite directions. In the rest of the production time, the sensible heat consistently contributed more than 95% of the total heat supplement, while that proportion of heat convection was less than 5%. Meanwhile, the contribution of heat conduction was negligible because the proportion was not more than 0.2% in the entire production test. After a 24-h gas production, a noteworthy change occurred, and the heat proportion of sensible heat began to decline, while the heat convection and heat conduction exhibited an upward trend. As the hydrate dissociation absorbs heat immediately from the HBS, a moderate hydrate dissociation will bring about a moderate release of sensible heat. So, the change might result from the continuous temperature decline, which made hydrates dissociated less intensively (Kim et al., 1987; Song et al., 2015). This explanation is in agreement with the temperature records, which presented a rapid temperature decrease before 24 h and then had a relatively temperate descending trend.

To sum up, hydrate dissociation will mainly count on sensible heat of formation in a relatively long term; therefore, a hydrate reservoir with a high initial temperature is preferable for production. But with the formation temperature gradually declining to the equilibrium temperature, the spontaneous hydrate dissociation and corresponding heat absorption from HBS will become feeble. In this stage, heat convection may play an increasingly important role. As for the production strategy, these perceptions suggest that the formation temperature is the primary factor in terms of thermodynamics. It is reasonable to choose a reservoir with a higher temperature, even to artificially supply heat into the reservoir to facilitate and maintain hydrate dissociation. In addition, it is also a measure worthy of consideration to enhance heat convection in a certain stage to boost the hydrate dissociation and compensate for the degradation of formation heat release. There has been plenty of research investigating the techniques or schemes by implementing heat injection and hydraulic fracturing in the hydrate reservoir (Li X.-S. et al., 2012; Chen et al., 2014; Konno et al., 2016; Chen et al., 2017; Sun et al., 2021), by which we can carry out the enhanced recovery of hydrates. It is foreseeable that novel comprehensive and sophisticated production strategies or methods will emerge and come into play in the upcoming hydrate production.

## 4 CONCLUSION

In this study, we proposed a thermodynamic method for the estimation of free gas proportion in a hydrate reservoir using the field production and monitoring data. Based on this, we managed to approximately estimate the free gas content in the first test reservoir in the Nankai Trough. Considering the main contributing thermal processes for hydrate dissociation,

namely, heat convection of formation water, heat conduction in formation, and sensible heat releasing of the thermal disturbed zone, we calculated the total heat consumption due to hydrate dissociation during the entire production period. We converted this heat consumption into equivalent hydrate-released gas according to the enthalpy of hydrate dissociation and obtained the estimated gas volume of 98356 m<sup>3</sup>, which means the proportion of free gas in total produced gas, or in total reservoir-trapped gas, may be 17.35%, as the actual total gas production was 119000 m<sup>3</sup>. Given the variation range of sensible heat, the lower and upper free gas proportions were estimated as 8.77% and 26.02%, respectively.

Based on the calculation results, the hydrate gas proportion varying with time indicates that free gas accounted for a major part of gas generation in the first few hours, and then the hydrate dissociation sprang up. The proportion exceeding 100% implies a delay of gas extraction due to sluggish gas migration in low-permeability formation. The subsequent decline of hydrate gas proportion and generation may imply a pause of hydrate dissociation and even reformation of hydrates.

The heat analyses demonstrated that hydrate dissociation was mainly contributed by the sensible heat of the disturbed zone at least in this 6-day production. Gas production related to sensible heat accounted for 95% or so of the total hydrate-released gas, while that of heat convection was less than 5% and not more than 0.2% for heat conduction.

Through thermodynamic analysis and calculation, we revealed the gas composition in a hydrate reservoir, which is essential for understanding and predicting the gas production behavior of the hydrate reservoir. The analysis of thermal response unraveled the energy contribution of different heat sources to hydrate dissociation, which will guide the development of the production strategy in the future.

## REFERENCES

- Boswell, R., and Collett, T. S. (2011). Current Perspectives on Gas Hydrate Resources. *Energy Environ. Sci.* 4 (4), 1206–1215. doi:10.1039/c0ee0203h
- Boswell, R., Myshakin, E., Moridis, G., Konno, Y., Collett, T. S., Reagan, M., et al. (2019). India National Gas Hydrate Program Expedition 02 Summary of Scientific Results: Numerical Simulation of Reservoir Response to Depressurization. *Mar. Pet. Geology*. 108, 154–166. doi:10.1016/j.marpetgeo.2018.09.026
- Chen, L., Feng, Y., Okajima, J., Komiya, A., and Maruyama, S. (2018). Production Behavior and Numerical Analysis for 2017 Methane Hydrate Extraction Test of Shenhu, South China Sea. *J. Nat. Gas Sci. Eng.* 53 (53), 55–66. doi:10.1016/j.jngse.2018.02.029
- Chen, L., Sasaki, H., Watanabe, T., Okajima, J., Komiya, A., and Maruyama, S. (2017). Production Strategy for Oceanic Methane Hydrate Extraction and Power Generation with Carbon Capture and Storage (CCS). *Energy* 126, 256–272. doi:10.1016/j.energy.2017.03.029
- Chen, Z., Feng, J., Li, X., Zhang, Y., Li, B., and Lv, Q. (2014). Preparation of Warm Brine *In Situ* Seafloor Based on the Hydrate Process for Marine Gas Hydrate Thermal Stimulation. *Ind. Eng. Chem. Res.* 53 (36), 14142–14157. doi:10.1021/ie501181r
- Clennell, M. B., Hovland, M., Booth, J. S., Henry, P., and Winters, W. J. (1999). Formation of Natural Gas Hydrates in marine Sediments: 1. Conceptual Model of Gas Hydrate Growth Conditioned by Host Sediment Properties. *J. Geophys. Res.* 104 (B10), 22985–23003. doi:10.1029/1999jb900175

## DATA AVAILABILITY STATEMENT

The raw data supporting the conclusion of this article will be made available by the authors, without undue reservation.

## AUTHOR CONTRIBUTIONS

SL: conceptualization, methodology, formal analysis, investigation, supervision, project administration, and funding acquisition. YS: conceptualization, methodology, formal analysis, investigation, data curation, writing–original draft, and visualization. CL: investigation, review and editing, and funding acquisition. WC: formal analysis, investigation, and review and editing. LC: review and editing. SML: formal analysis and review and editing. XL: supervision, project administration, and funding acquisition. All authors contributed to manuscript revision and read and approved the submitted version.

## FUNDING

This study was funded by the Guangdong Major Project of Basic and Applied Basic Research (No. 2020B0301030003), the National Natural Science Foundation of China (42090023 and 51991365), China Geological Survey Project (No. DD20211350), the IGGCAS Key Deployment Project (Nos. IGGCAS-201903 and SZJJ201901), the Key Deployment Program of Chinese Academy of Sciences (Nos. YJKYYQ20190043, ZDBS-LY-DQC003, XDA14040401, KFZD-SW-422, and ZDRW-ZS-2021-3-1), and the CAS Key Technology Talent Program.

- Cortes, D. D., Martin, A. I., Yun, T. S., Francisca, F. M., Santamarina, J. C., and Ruppel, C. (2009). Thermal Conductivity of Hydrate-Bearing Sediments. *J. Geophys. Res.* 114 (B11). doi:10.1029/2008jb006235
- Feng, Y., Chen, L., Suzuki, A., Kogawa, T., Okajima, J., Komiya, A., et al. (2019). Enhancement of Gas Production from Methane Hydrate Reservoirs by the Combination of Hydraulic Fracturing and Depressurization Method. *Eng. Convers. Management* 184, 194–204. doi:10.1016/j.enconman.2019.01.050
- Fujii, T., Suzuki, K., Takayama, T., Tamaki, M., Komatsu, Y., Konno, Y., et al. (2015). Geological Setting and Characterization of a Methane Hydrate Reservoir Distributed at the First Offshore Production Test Site on the Daini-Atsumi Knoll in the Eastern Nankai Trough, Japan. *Mar. Pet. Geology*. 66, 310–322. doi:10.1016/j.marpetgeo.2015.02.037
- Handa, Y. P. (1986). Compositions, Enthalpies of Dissociation, and Heat Capacities in the Range 85 to 270 K for Clathrate Hydrates of Methane, Ethane, and Propane, and Enthalpy of Dissociation of Isobutane Hydrate, as Determined by a Heat-Flow Calorimeter. *The J. Chem. Thermodynamics* 18 (10), 915–921. doi:10.1016/0021-9614(86)90149-7
- Haynes, W. M. (2016). *CRC Handbook of Chemistry and Physics*. 97th Edition. Boca Raton: Taylor and Francis/CRC Press.
- Kim, H. C., Bishnoi, P. R., Heidemann, R. A., and Rizvi, S. S. H. (1987). Kinetics of Methane Hydrate Decomposition. *Chem. Eng. Sci.* 42 (7), 1645–1653. doi:10.1016/0009-2509(87)80169-0
- Konno, Y., Fujii, T., Sato, A., Akamine, K., Naiki, M., Masuda, Y., et al. (2017). Key Findings of the World's First Offshore Methane Hydrate Production Test off the Coast of Japan: Toward Future Commercial Production. *Energy Fuels* 31 (3), 2607–2616. doi:10.1021/acs.energyfuels.6b03143



- Konno, Y., Jin, Y., Yoneda, J., Uchiumi, T., Shinjou, K., and Nagao, J. (2016). Hydraulic Fracturing in Methane-Hydrate-Bearing Sand. *RSC Adv.* 6 (77), 73148–73155. doi:10.1039/c6ra15520k
- Konno, Y., Masuda, Y., Hariguchi, Y., Kurihara, M., and Ouchi, H. (2010). Key Factors for Depressurization-Induced Gas Production from Oceanic Methane Hydrates. *Energy Fuels* 24 (3), 1736–1744. doi:10.1021/ef901115h
- Kvenvolden, K. A. (1988). Methane Hydrate — A Major Reservoir of Carbon in the Shallow Geosphere? *Chem. Geology*. 71 (1), 41–51. doi:10.1016/0009-2541(88)90104-0
- Li, G., Li, B., Li, X.-S., Zhang, Y., and Wang, Y. (2012a). Experimental and Numerical Studies on Gas Production from Methane Hydrate in Porous Media by Depressurization in Pilot-Scale Hydrate Simulator. *Energy Fuels* 26 (10), 6300–6310. doi:10.1021/ef301229k
- Li, X.-S., Wang, Y., Duan, L.-P., Li, G., Zhang, Y., Huang, N.-S., et al. (2012b). Experimental Investigation into Methane Hydrate Production during Three-Dimensional thermal Huff and Puff. *Appl. Energy*. 94, 48–57. doi:10.1016/j.apenergy.2012.01.024
- Li, X.-S., Xu, C.-G., Zhang, Y., Ruan, X.-K., Li, G., and Wang, Y. (2016). Investigation into Gas Production from Natural Gas Hydrate: A Review. *Appl. Energy*. 172, 286–322. doi:10.1016/j.apenergy.2016.03.101
- Lu, X., Zhang, X., Wang, P., and Liang, Q. (2019). Advances of Formation Dynamics of Natural Gas Hydrate. *Sci. Sin.-Phys. Mech. Astron.* 49 (3), 034605. doi:10.1360/sspma2018-00362
- Makogon, Y. F., and Omelchenko, R. Y. (2013). Commercial Gas Production from Messoyakha deposit in Hydrate Conditions. *J. Nat. Gas Sci. Eng.* 11, 1–6. doi:10.1016/j.jngse.2012.08.002
- Miyakawa, A., Saito, S., Yamada, Y., Tomaru, H., Kinoshita, M., and Tsuji, T. (2014). Gas Hydrate Saturation at Site C 0002, IODP Expedition 314 and 315, in the K Umano B Asin, Nankai Trough. *Isl. Arc* 23 (2), 142–156. doi:10.1111/iar.12064
- Moridis, G. J., Collett, T. S., Boswell, R., Kurihara, M., Reagan, M. T., Koh, C., et al. (2009). Toward Production from Gas Hydrates: Current Status, Assessment of Resources, and Simulation-Based Evaluation of Technology and Potential. *Spe Reservoir Eval. Eng.* 12 (5), 745–771. doi:10.2118/114163-pa
- Moridis, G. J., Kowalsky, M. B., Pruess, K., and Lawrence Berkeley Nat, L. (2005). Depressurization-Induced Gas Production from Class-1 Hydrate Deposits. *Spe Reservoir Eval. Eng.* 10 (5), 458–481. doi:10.2118/97266-MS
- Muraoka, M., Ohtake, M., Suzuki, N., Yamamoto, Y., Suzuki, K., and Tsuji, T. (2014). Thermal Properties of Methane Hydrate-Bearing Sediments and Surrounding Mud Recovered from Nankai Trough wells. *J. Geophys. Res. Solid Earth* 119 (11), 8021–8033. doi:10.1002/2014jb011324
- Sharqawy, M. H., Lienhard, J. H., and Zubair, S. M. (2012). Thermophysical Properties of Seawater: a Review of Existing Correlations and Data. *Desalination Water Treat.* 16 (1-3), 354–380. doi:10.5004/dwt.2010.1079
- Sloan, E. D. (2003). Fundamental Principles and Applications of Natural Gas Hydrates. *Nature* 426 (6964), 353–359. doi:10.1038/nature02135
- Sloan, E. D., and Koh, C. A. (2008). *Clathrate Hydrates of Natural Gases*. Boca Raton, FL: CRC Press.
- Song, Y., Cheng, C., Zhao, J., Zhu, Z., Liu, W., Yang, M., et al. (2015). Evaluation of Gas Production from Methane Hydrates Using Depressurization, thermal Stimulation and Combined Methods. *Appl. Energy*. 145, 265–277. doi:10.1016/j.apenergy.2015.02.040
- Sun, Y., Li, S., Lu, C., Liu, S., Chen, W., and Li, X. (2021). The Characteristics and its Implications of Hydraulic Fracturing in Hydrate-Bearing Clayey silt. *J. Nat. Gas Sci. Eng.* 95, 104189. doi:10.1016/j.jngse.2021.104189
- Waite, W. F., Santamarina, J. C., Cortes, D. D., Dugan, B., Espinoza, D. N., Germaine, J., et al. (2009). Physical Properties of Hydrate-Bearing Sediments. *Rev. Geophys.* 47 (4). doi:10.1029/2008rg000279
- Waite, W. F., Stern, L. A., Kirby, S. H., Winters, W. J., and Mason, D. H. (2007). Simultaneous Determination of thermal Conductivity, thermal Diffusivity and Specific Heat in sl Methane Hydrate. *Geophys. J. Int.* 169 (2), 767–774. doi:10.1111/j.1365-246X.2007.03382.x
- Xu, T., Zhang, Z., Li, S., Li, X., and Lu, C. (2021). Numerical Evaluation of Gas Hydrate Production Performance of the Depressurization and Backfilling with an *In Situ* Supplemental Heat Method. *ACS Omega* 6 (18), 12274–12286. doi:10.1021/acsomega.1c01143
- Xu, W., and Ruppel, C. (1999). Predicting the Occurrence, Distribution, and Evolution of Methane Gas Hydrate in Porous marine Sediments. *J. Geophys. Res.* 104 (B3), 5081–5095. doi:10.1029/1998jb900092
- Yamamoto, K., Kanno, T., Wang, X.-X., Tamaki, M., Fujii, T., Chee, S.-S., et al. (2017). Thermal Responses of a Gas Hydrate-Bearing Sediment to a Depressurization Operation. *RSC Adv.* 7 (10), 5554–5577. doi:10.1039/C6RA26487E
- Yamamoto, K., Terao, Y., Fujii, T., Ikawa, T., and Seki, M. (2014). “Operational Overview of the First Offshore Production Test of Methane Hydrates in the Eastern Nankai Trough,” in *Offshore Technology Conference 2014* (Houston, Texas, USA: OnePetro). doi:10.4043/25243-ms
- Yang, L., Zhao, J., Liu, W., Yang, M., and Song, Y. (2015). Experimental Study on the Effective thermal Conductivity of Hydrate-Bearing Sediments. *Energy* 79, 203–211. doi:10.1016/j.energy.2014.11.008
- Yang, L., Zhao, J., Wang, B., Liu, W., Yang, M., and Song, Y. (2016). Effective thermal Conductivity of Methane Hydrate-Bearing Sediments: Experiments and Correlations. *Fuel* 179, 87–96. doi:10.1016/j.fuel.2016.03.075
- Ye, J.-l., Qin, X.-w., Xie, W.-w., Lu, H.-l., Ma, B.-j., Qiu, H.-j., et al. (2020). The Second Natural Gas Hydrate Production Test in the South China Sea. *China Geology*. 3, 197–209. doi:10.31035/cg2020043
- Yu, T., Guan, G., and Abudula, A. (2019). Production Performance and Numerical Investigation of the 2017 Offshore Methane Hydrate Production Test in the Nankai Trough of Japan. *Appl. Energy*. 251, 113338. doi:10.1016/j.apenergy.2019.113338

**Conflict of Interest:** The authors declare that the research was conducted in the absence of any commercial or financial relationships that could be construed as a potential conflict of interest.

**Publisher’s Note:** All claims expressed in this article are solely those of the authors and do not necessarily represent those of their affiliated organizations, or those of the publisher, the editors and the reviewers. Any product that may be evaluated in this article, or claim that may be made by its manufacturer, is not guaranteed or endorsed by the publisher.

Copyright © 2022 Li, Sun, Lu, Chen, Liu, Chen and Li. This is an open-access article distributed under the terms of the Creative Commons Attribution License (CC BY). The use, distribution or reproduction in other forums is permitted, provided the original author(s) and the copyright owner(s) are credited and that the original publication in this journal is cited, in accordance with accepted academic practice. No use, distribution or reproduction is permitted which does not comply with these terms.